International Journal of Engineering Sciences & Research Technology

(A Peer Reviewed Online Journal)
Impact Factor: 5.164

IJESRT

RESEARCHERID
THOMSON REUTERS

[Ekott *et al.*, 12(7): July, 2023]
IC™ Value: 3.00

ISSN: 2277-9655
Impact Factor: 5.164
CODEN: IJESS7

IJESRT

INTERNATIONAL JOURNAL OF ENGINEERING SCIENCES & RESEARCH TECHNOLOGY

MOLECULAR DYNAMICS, CRACK PROPAGATION ON THE 10*10*10 STRUCTURE OF TYPE B2 TIAL, PARIS LAW

Alain DZABANA HONGUELET[*1,2,4], Charlemagne Guy Franklin MOUSSOKI YENGO[2,4,5], Georges Désiré BIDILOU [2,4,5], Timothée NSONGO[1,2,3]

[1]Faculty of Science and Technology, Marien Ngouabi University, Congo Brazzaville
[2]Research Group on the Physical and Chemical Properties of Materials, Congo Brazzaville
[3]Centre for Geological and Mining Research, Congo Brazzaville
[4]Association Alpha Sciences Beta Technologies, Congo Brazzaville
5Ecole Normale Supérieure, Congo Brazzaville.

DOI: 10.5281/zenodo.8116175

ABSTRACT

In this work, we observed the crack propagation on a 10*10*10 TiAl structure of type B2 with a mesh parameter of 2.824 A; molecular dynamics simulation incorporated in the LAMMPS calculation code with the use of the MEAM potential. To do this, we applied a uniaxial voltage with a maximum value of 30KN along the oz axis for 60s. After several balancing steps, we empirically followed the crack propagation mode according to the Paris law.

The TiAl MEAM potential used in this work allowed us to calculate the cohesive energies of different TiAl structures. It was shown that the Type B2 structure is intermediate with a cohesive energy of -4.375eV and a cubic lattice parameter of 3.23A.

During equilibration, for the first 30s, we monitored the behaviour of the physical quantities around 300K: kinetic and potential energies, showing overall stable behaviour around the last 20 seconds.

Deformation was observed between 30 and 60s at around 300 K. This deformation is the result of the progressive application of stress along the oz axis; pressure is the main physical parameter exploited during this deformation, as is the depth of cracking observed along the oy axis.

The evolution of the depth along Oy allowed us to empirically follow the regime mode of the crack propagation, for which we fixed the parameter c=3.5 10-9 , for m=1, we showed that the regime curve is close to the Paris law.

Keywords: Molecular dynamics, crack propagation, Paris law, MEAM potential, deformation, LAMMPS.

1. INTRODUCTION

Fracture is an integral part of our daily lives, and is therefore a problem that man will have to contend with for as long as he remains on earth and continues to construct buildings and mechanical structures. It's a problem that is becoming increasingly interesting as science and technology evolve.

Advances in our knowledge of fracture mechanics have made it possible today, and more specifically since the middle of the 20th century, to better prevent the risk of fracture. However, many failure mechanisms are still poorly understood, particularly when new materials or processes are used. According to economic studies carried out since the early 1980s, the cost of catastrophic failures represents almost 4% of GNP in developed industrial countries. This cost can be reduced by around 30% by applying breakthrough studies correctly, and by a further 25% by further developing research in the field of breakthroughs.

It is no longer refutable that all mechanical parts contain cracks that are observable to the naked eye (cracks linked to the use of a new material or process) and cracks that are not observable to the naked eye (cracks

ISSN: 2277-9655
Impact Factor: 5.164
CODEN: IJESS7

caused by negligence in the design and use of the structure). It is therefore essential to study cracks and understand how they move in order to avoid a number of disasters.

Marine structures such as ships, submarines and oil rigs are naturally subjected to variable (cyclical) stresses over time which, although below the material's elastic limit, can lead to failure when applied a large number of times: this is the process of fatigue damage.

The use of steels, now widely employed in shipbuilding, means that their resistance to fatigue must be taken into account in the design rules. Despite the periodic checks carried out on these parts in service, it is sometimes difficult to identify the phenomenon of fatigue, which is very slow and allows a crack to propagate to a critical value. Structural fatigue is particularly insidious because of its progressive, hidden nature. This behaviour is all the more serious because fatigue cracking very often leads to sudden failure, which can cause an accident.

Recent events illustrate the disastrous consequences that fatigue failure can have on a ship or offshore platform (Prestige, Erika, Alexander Kielland...) and remind us of the importance of developing research into understanding the mechanisms involved in the fatigue phenomenon and studying the main factors influencing the speed at which fatigue cracks propagate.

Controlling the phenomenon of fatigue is therefore of paramount importance, since it affects the safety of structures in normal operation, subject to loads that vary over time, as well as other factors such as the aggressiveness of the environment, which can accelerate their reduction in fatigue strength and consequently lead to failure.

In Congo Brazzaville, the Groupe de Recherche sur les Propriétés Physiques et Chimiques des Matériaux (Research Group on the Physical and Chemical Properties of Materials) has been working on Ti-Al for a number of years, making it an exciting subject for development. Professor Timothée NSONGO studied the order-disorder transformation of the TiAl binary alloy system by numerical simulation using the EAM inserted atom method. The aim of his thesis was mainly to determine the influence of the lattice constant and composition on the type of order-disorder transformation and the order process in the alloys.

Mr. MIMBOUI Yhann, still in the same section, is working on Titanium alloys. Part of his work is on order transitions in short-range Ti-Al after having made a prediction in L10 of the Ti-Al structure.

However, the use of an alloy depends on its resistance to external stresses. It is with this objective in mind that this study was carried out to investigate the reaction of Ti-Al under different loads.

The aim of this project is to simulate the effect of stress-strain under crack propagation using MEAM potentials in a 10*10*10 TiAl B2 structure. As this alloy is widely used in the aerospace and transport sectors because of its special properties, it seems interesting to study crack propagation in this alloy.

2. MATERIALS AND METHODS

II 1 Molecular dynamics

Molecular Dynamics is a formidable tool for investigating matter at the atomic scale. It involves numerically simulating the evolution of a system of particles as a function of time, with the aim of predicting and understanding experimental results. It makes it possible to highlight structural arrangements or dynamic phenomena that are still inaccessible to current experimental observation methods (EXAFS, NMR, Atom Probe Tomography - APT), especially for amorphous materials such as glasses. This move into the digital world requires time to be discretised in order to solve Newton's equations governing the motion of each particle. The principle of Molecular Dynamics is then to integrate these discretised equations, under various physical constraints, using various algorithms which can be found in various reference books such as that by Griebel et al.12 , a clear work containing examples and practical applications, useful for anyone wanting to start writing their own Molecular Dynamics programme. The methods presented are those used in this thesis. After an explanation of the "Velocity-Störmer-Verlet" algorithm, which strikes a balance between robustness, practicality and performance, a presentation of the Nosé-Hoover thermostat and barostat shows how the temperature and pressure of a material can be controlled in a fully integrated way. A key point in the simulations is the

ISSN: 2277-9655
Impact Factor: 5.164
CODEN: IJESS7

appropriate parameterisation of interatomic interactions. The interaction potential used must above all take account of known properties in order to be able to predict those that are not, or to be able to explain a phenomenon that is still poorly understood[1]. Calculating these interactions during simulation, particularly electrostatic interactions, is the step that requires the most numerical computing resources. The method developed by Wolf overcomes this limitation and opens up the field of simulations on much larger size and time scales. These methods and algorithms are finally being applied to the modelling of silica materials, in particular glasses, where certain properties and experimental behaviours are reproduced with acuity.

II 1 a Algorithms for integrating Newton's equations [1].

In Classical Molecular Dynamics, each particle is considered as a point mass interacting at a distance with others via an effective interaction potential. In an ensemble of N interacting particles, the motion of particle i of mass m_i (with i = 1 to N) is governed by the equation :

$$m_i \frac{d^2 x_i}{dt^2} = F_i \qquad (1)$$

with the convention $x_i = \overrightarrow{x_i}$ for the position vector, and F_i is the vector resulting from all the forces applied to particle i.

II 1 b Standard Störmer-Verlet method [1].

The basic numerical method for solving the equations of motion is to perform a 3rd order Taylor series expansion of the position x around the date t, i.e. at $t \pm \delta t$ (with δt small):

$$\begin{cases} x(t+\delta t) = x(t) + \delta t \frac{dx}{dt} + \frac{1}{2}\delta t^2 \frac{d^2x}{dt^2} + \frac{1}{6}\delta t^3 \frac{d^3x}{dt^3} \\ x(t-\delta t) = x(t) - \delta t \frac{dx}{dt} + \frac{1}{2}\delta t^2 \frac{d^2x}{dt^2} - \frac{1}{6}\delta t^3 \frac{d^3x}{dt^3} \end{cases} \qquad (2)$$

By adding up and grouping the terms, we obtain :

$$\frac{d^2x}{dt^2} = \frac{1}{\delta t^2}[x(t+\delta t) - 2x(t) + x(t-\delta t)] \qquad (3)$$

Time is discretised using a time step δt (of the order of femto seconds in Molecular Dynamics). At iteration n, the date is expressed by $t_n = n\delta t$, the position vector by x_i^n, the velocity vector by v_i^n and the force vector by F_i^n. After this discretisation and digitisation, the previous equation becomes, for the date $t_{n+1} = t_n + \delta t$:

$$m_i \frac{1}{\delta t^2}(x_i^{n+1} - 2x_i^n + x_i^{n-1}) = F_i^n \qquad (4)$$

In the same way, but subtracting the terms this time, we obtain the expression for speed :

$$\frac{d^2x}{dt^2} = \frac{x(t+\delta t) - x(t-\delta t)}{2\delta t} = v_i^n = \frac{x_i^{n+1} - x_i^{n-1}}{2\delta t} \qquad (5)$$

This is the standard form of the Störmer-Verlet method for integrating Newton's equations:

$$\begin{cases} x_i^{n+1} = 2x_i^n - x_i^{n-1} + \frac{\delta t^2}{m_i} F_i^n \\ v_i^n = \frac{x_i^{n+1} - x_i^{n-1}}{2\delta t} \end{cases} \qquad (6)$$

II 2 Potentials and the MEAM method [1]

A material is modelled by choosing and setting parameters for an interatomic potential, from which are derived the forces interacting between the different particles present in the simulation box. This is usually an effective

ISSN: 2277-9655
Impact Factor: 5.164
CODEN: IJESS7

potential. Its parameters are set in such a way that the effects of the model reproduce known properties of the material being simulated (crystalline structures, elastic properties, X-ray diffraction pattern, infrared spectrum, NMR, etc.). A correctly parameterised interaction potential is crucial for predicting or accurately interpreting as yet unexplained properties of the modelled material. The MEAM potential of the Ti-Al alloy was used in our work.

II 2 a Modified incorporated atom method [2]

Interatomic potentials are of vital importance for simulations that model the properties of materials. The basis of these potentials is Density Function Theory (DFT), which postulates that energy is a function of electron density. By knowing the electron density of an entire system, we can determine the potential energy of a system:

$$U = [\rho(r)] \tag{7}$$

$$E[\rho(r)] = \mathrm{Ts}[\rho(r)] + \mathrm{J}[\rho(r)] + \mathrm{Exc}[\rho(r)] + \mathrm{Eext}[\rho(r)] + \mathrm{E}_{ii}\,[\rho(r)] \tag{8}$$

where E is the total energy, Ts is the kinetic energy of the single particle, J is the Hartree electron-electron energy, Exc is the exchange correlation function, Eext is the electron-ion coulombic interaction, and E_{ii} is the ion-ion energy.

On this basis, the Embedded Atom Method (EAM) was created by assuming that an atom can be embedded in a homogeneous electron gas and that the change in potential energy is a function of the electron density of the embedded atom which can be approximated by an embedding function. In a crystal, however, the electron density is not homogeneous, so the EAM potential replaces the background electron density with the electron densities of each atom and supplements the embedding energy with a repulsive pair potential to represent the core-core interactions of the atoms.

With a simple linear superposition of the electron densities of the atoms as the background electron density, the EAM is governed by the following equations:

$$\mathrm{R}_{ii} = |r_i - r_j| \tag{9}$$

$$\bar{\rho}_i = \sum\left(\mathrm{R}_{ij}\right)_j \tag{10}$$

$$U = \sum(\bar{\rho}_i)_i + \frac{1}{2}\sum \emptyset\left(\mathrm{R}_{ij}\right)_{i,j} \tag{11}$$

Where R_{ij} is the distance between atoms i and j, $r_{i,j}$ is the position between atoms i and j, $\bar{\rho}_i$ is the fundamental electron density, and ϕ is the pair interaction potential.

However, EAM does not do an excellent job of simulating materials with significant directional binding, which includes most metals. In order to correctly simulate metals, the modified embedded atom method was created, which allows the background electron density to depend on the local environment instead of assuming a linear superposition.

In the MEAM formalism, we consider a set of atoms forming a cluster. Each atom is immersed in the electron density created by the other atoms. The total energy depends on two factors: the immersion potential and the pair interaction potential:

$$E = \sum_i F_i(\bar{\rho}_i) + \frac{1}{2}\sum_{j\neq 1} \phi_{ij}(R_{ij}) \tag{12}$$

For an atom i,
F_i is the immersion potential,
$\bar{\mathrm{n}}_i$ is the fundamental electron density.
$\phi_{ij}(R_{ij})$ is the pair interaction potential between two atoms i and j, at distance R_{ij}.

The immersion potential is calculated as follows:

ISSN: 2277-9655
Impact Factor: 5.164
CODEN: IJESS7

$$F_i(\bar{\rho}_i) = AE_c \frac{\bar{\rho}_i}{\rho_0} Ln(\frac{\bar{\rho}_i}{\rho_0}) \quad (13)$$

where :
A is a parameter that can be adjusted according to the experimental data;
E_c *is the sublimation energy :*
ρ_0 *the electron density in the reference structure ;*
$\bar{\rho}_i$ *the electron density in the real structure.*

In MEAM1, interactions in the reference structure are limited to the first neighbourhood. Under these conditions, the atomic positions and bond directions are fixed. The immersion potential depends only on the distance to the first neighbourhood and the number of first neighbours. Consequently, the energy of an atom can be written as a function of R as follows:

$$E^u(R) = F\left[\bar{\rho}_i{}^0(R)\right] + \frac{Z_1}{2}\phi(R) \quad (14)$$

where Z_1 *is the number of first neighbours of the atom.*

By calculating $E^u(R)$ from Rose's equation of state, we can derive the expression for the interaction potential of the pairs as follows:

$$\phi(R) = \frac{2}{Z_1}[E^u(R) - F\left[\bar{\rho}_i{}^0(R)\right]] \quad (15)$$

In MEAM2, we consider second-neighbour interactions in the reference structure and this can be done by adding a screen parameter S. From this, the energy of an atom in a reference structure can then be written :

$$E^u(R) = F\left[\bar{\rho}_i{}^0(R)\right] + \frac{Z_1}{2}\phi(R) + \frac{Z_2 S}{2}\phi(aR) \quad (16)$$

where :
Z_1 *is the number of first neighbours in the reference structure ;*
Z_2 *is the number of second neighbours in the reference structure ;*
a is the ratio of the distances of the second and first neighbours $a=R_2/R_1$ *;*
S is the screen function. For a given reference structure, the screen factor S is constant.

The above equation can be written as :

$$E^u(R) = F\left[\bar{\rho}_i{}^0(R)\right] + \frac{Z_1}{2}\psi(R) \quad (17)$$

with $$\psi(R) = \phi(R) + \frac{Z_2 S}{Z_1}\phi(aR) \quad (18)$$

From the value $\psi(R)$ the pair interaction potential is calculated iteratively using the following formula :

$$\phi(R) = \psi(R) + \sum_{n=1}(-1)^n(\frac{Z_2 S}{Z_1})^n \psi(a^n R) \quad (19)$$

For a MEAM interatomic potential that describes the relationship for alloys with two or more components, each component needs 13 individual adjustable parameters. In addition, each binary interaction requires at least 14 adjustable parameters. These parameters are used in the calculation of the potential energy described in equation (7) and govern the forces acting on the atoms. These parameters are shown below (see library: parameter)

The main difference between the potential energy equation for EAM and MEAM is the inclusion of S, which reflects the shielding effect.

ISSN: 2277-9655
Impact Factor: 5.164
CODEN: IJESS7

For a MEAM interatomic potential that describes the relationship for alloys with two or more components, each of the components needs 13 individual adjustable parameters. In addition, each binary interaction requires at least 14 adjustable parameters.

II 3 Betting law: Fatigue growth regimes for long cracks

The stress applied at the crack tip, through the region where the asymptotic fields of linear fracture mechanics dominate, can be characterised by the stress intensity factor [3]. The main physical mechanism leading to *crack extension is* cyclic *plastic deformation at the* crack tip. For this reason, in the early 1960s, Parus and Erdogan and Paris, Gomez and Anderson correlated the rate of fatigue cracking with the magnitude of the stress intensity factor [4].

The diagram (Figure 1), drawn in logarithmic coordinates, shows three regimes. A central regime (regime B), in which the cracking rate is proportional to the amplitude of the stress intensity factor at a power *m*. Values of *m* generally range from 2 to 4, or even 5 for alloys with low resistance to fatigue cracking.

In the case of the mild steel studied, *m is* found to be equal to 3.5. This regime is known as the Paris regime [4,3]. Beyond this, regime *C*, cracking velocities are greater than those predicted by the Paris law, and the crack propagates in an unstable manner for $K=K_c$. Below this, regime A, cracking speeds are lower than those predicted by the Paris law. When K decreases until the non-propagation threshold is reached, the cracking velocity decreases rapidly, and the crack appears to stop. [5]

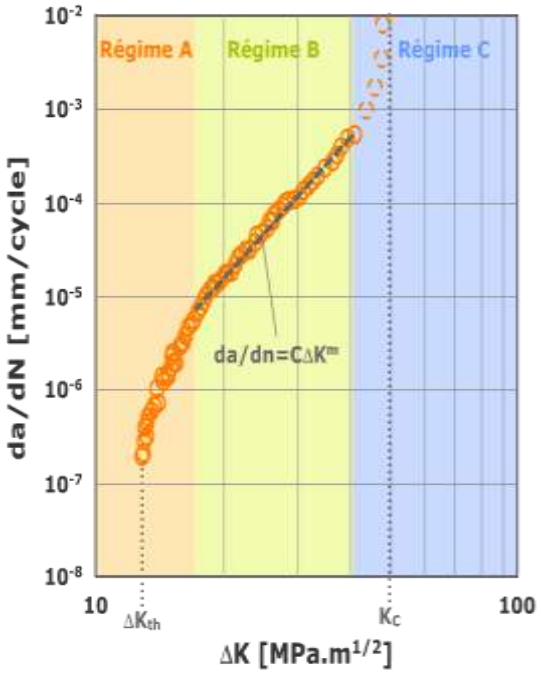

Figure 1: Vitesses de fissuration mesurées sur éprouvette CT,sur un acier doux à 0,38 % de carbone à température Ambient and R=0 [6], Illustration of the different fatigue propagation regimes. Paris law applies in regime

Depending on the behaviour of the material with respect to propagation and the direction of the imposed stress, physical quantities have been calculated in order to interpret the resulting phenomena. The physical quantity K has been the subject of several studies, but numerous other laws have been written which take into account either the factor R of the stress ratio, or the threshold value Ks and the toughness of the materialK1c.

For the study presented below, three distinct expressions have been selected for comparison with the experimental results to be obtained.

ISSN: 2277-9655
Impact Factor: 5.164
CODEN: IJESS7

- An initial empirical relationship proposed by G.T. Hahn in 1972 [7] when studying steels :

$$\frac{da}{dN} = C[\Delta K]^m \qquad (20)$$

II 3 Working procedure

In this work, we carried out a simulation of crack propagation under variable stress for a finite period of time. This work required the contribution of many elements such as the study structure, the MEAM potential of TiAl and also the setting of many parameters relating to the crack propagation mode. The principle is to calculate the strain for each stress.

II 3 a Validity of the MEAM potential: Structural properties of TiAl

The Ti-Al structure used in this work is of type B2 with a crystalline parameter of 2.824 A, found in the Materials Project database, a website that makes the results of several researchers, generally from the first principle, freely available.

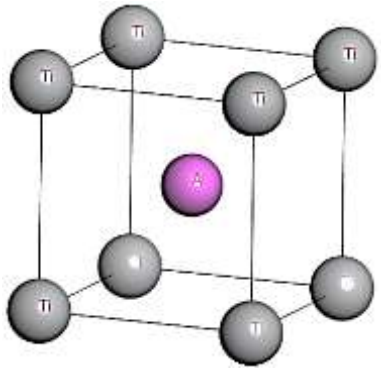

Figure 2: Ti-Al B2

Once we had obtained the crystallographic structure, we generated the data file specific to the LAMMPS calculation code using the OVITO software. This data file shows the number of atoms, the types of atoms, the mesh parameters and the atomic coordinates:

 # LAMMPS data file written by OVITO
2 atoms
2 atom types
0.0 2.824105 xlo xhi
0.0 2.824105 ylo yhi
0.0 2.824105 zlo zhi

Atoms # atomic

1 1 2.824105 2.824105 2.032356
2 2 0.0 0.0 0.0

For simulation purposes, we generated a 10x10x10 cell, i.e. a mesh of 2,000 atoms, using the AtomSK program.

II 3 b MEAM potential Ti-Al

Potentials are essential for studying the physical properties of systems, but some potentials do not interpret certain phenomena in certain cases. For our study, we opted instead for the MEAM potential, an evolved version of the EAM potential whose parameters are divided into two parts: library and interaction parameters [8].

ISSN: 2277-9655
Impact Factor: 5.164
CODEN: IJESS7

Parameters - Library :

This is the set of potential parameters of each of the composite elements of the Ti-Al alloy separately in their original structures.

```
#elt lat z iel atwt
# alpha b0 b1 b2 b3 alat esub asub
# t0 t1 t2 t3 rozero ibar

Al' 'fcc' 12 0 26.9820
        4.6855976824 3.2000 2.6000 6.0000 2.6000 4.0446507884 3.3600 1.1600
    1.0000 3.0500 0.5100 7.7500 1.0000 3

Ti' 'hcp' 12 0 47.8800
        4.7194566335 2.7000 1.0000 3.0000 1.0000 2.9200000000 4.8700 0.6600
```

Parameters-interaction :

These parameters define all the interactions of the elements pooled in the new structure; in our case, Ti and Al in structure B2.

rc = 4.8	zbl(1,1) = 0	zbl(1,2) = 0	zbl(2,2) = 0	Cmin(1,1,2) = 0.4900
delr = 0.1	nn2(1,1) = 1	nn2(1,2) = 1	nn2(2,2) = 1	Cmin(2,2,1) = 1.3000
augt1 = 0	rho0(1) = 1.0000	lattce(1,2) = 'b2	rho0(2) = 1.0000	Cmin(1,2,1) = 0.7225
erose_form = 2	Ec(1,1) = 3.3600	Ec(1,2) = 4.3750	Ec(2,2) = 4.8700	Cmin(2,1,1) = 0.7225
ialloy = 2	re(1,1) = 2.8600	re(1,2) = 2.8000	re(2,2) = 2.9200	Cmin(1,2,2) = 0.4600
	alpha(1,1) = 4.68559768	alpha(1,2) = 5.56259868	alpha(2,2) = 4.71945663	Cmin(2,1,2) = 0.4600
	repuls(1,1) = 0.0500	repuls(1,2) = 0.0250	repuls(2,2) = 0.0000	Cmax(1,1,2) = 1.4400
	attrac(1,1) = 0.0500	attrac(1,2) = 0.0250	attrac(2,2) = 0.0000	Cmax(2,2,1) = 2.8000
	Cmin(1,1,1) = 0.4900		Cmin(2,2,2) = 1.0000	Cmax(1,2,1) = 2.8000
	Cmax(1,1,1) = 2.8000		Cmax(2,2,2) = 1.4400	Cmax(2,1,1) = 2.8000
				Cmax(1,2,2) = 1.4400
				Cmax(2,1,2) = 1.4400

There is a whole database of potential pairs available on the www.nist.gov website.

II 3 c Crack and propagation mode

The propagation studied here uses the betting law for the case of a semi-infinite plate containing a deep crack placed on (oy) subjected to a uniaxial stress on (oz).

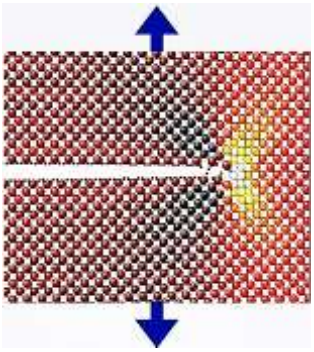

Barsom and Rolfe in their studies on structural steel showed that :

ISSN: 2277-9655
Impact Factor: 5.164
CODEN: IJESS7

$$\frac{da}{dN} = C[\Delta K]^m \quad (21)$$

where C=6.9 10^{-9} for the upper limit and C=3.45 10^{-9} for the lower limit in structural steels.

For a semi-infinite plate containing a lateral crack of depth b subjected to a homogeneous uniaxial stress σ we have

$$K = 1.222\sigma\sqrt{\pi a} \quad (22)$$

We set the parameter "C" at 3.45 10^{-9} and empirically represented the cracking curve for different values of m less than 4.

3. RESULTS AND DISCUSSION

The results are presented here in a systematic way, firstly for the choice of the MEAM potential, then for all the stages of the phenomenon observed, in particular balancing, deformation or application of the stress and finally the treatment according to the betting law.

III 1 Validity of the MEAM potential: Structural properties

For the choice of potential, we tested several structures of the Ti-Al alloy; for these different structures, we calculated their cohesive energies, which we present in the table below.

-Cohesive energy and mesh parameters :

We calculated the cohesion energies in different crystallographic structures for TiAl; we found that the Do19 structure is the most stable with a cohesion energy of -4.766eV followed by the Do22 structure with a cohesion energy of -4.64eV and in last place the B1 structure with an energy of -3.92eV.

Table 1: Cohesive energy per Ti-Al structure

Structures	Parameters a(Å)	Total energy(ev)	Ecoh(ev)	Number of atoms
TiAl (L $)_{10}$	**4.02**	**-17.53**	**-4.38**	**4**
TiAl(B1)	**5.44**	**-31.32**	**-3.92**	**8**
TiAl(B2)	**3.23**	**-8.749**	**-4.375**	**2**
Ti_3 Al(Do $)_{19}$	**5.75**	**-38.128**	**-4.766**	**8**
$TiAl_3$ (Do $)_{22}$	**3.94**	**-37.15**	**-4.64**	**8**

Although the number of atoms per mesh increases in certain structures, the cohesive energy becomes very high, reflecting the instability of the structure below eight (8) atoms per mesh.

ISSN: 2277-9655
Impact Factor: 5.164
CODEN: IJESS7

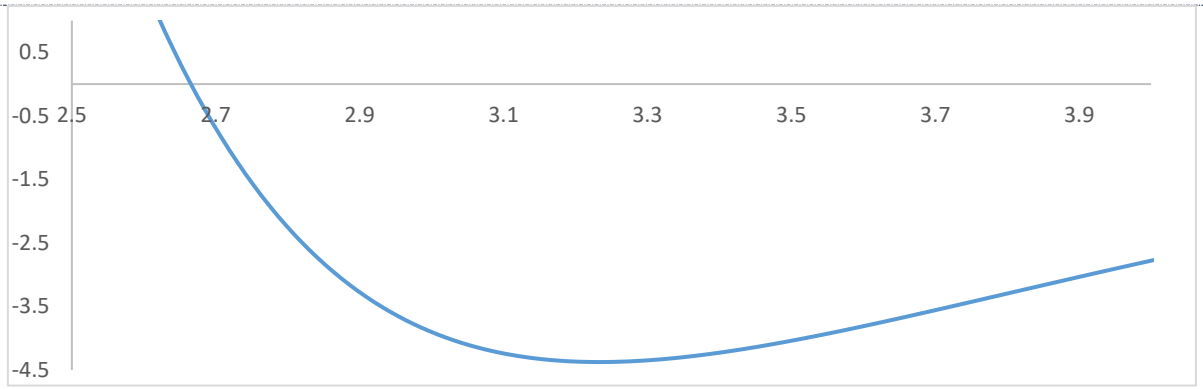

Figure 4: Structural cohesive energy B2

III 2 Propagation phenomenon :

We show here all the results obtained at different stages of crack propagation. First, the observation lasts 1 minute, the first thirty seconds are devoted to equilibration, then the last thirty seconds are devoted to observing the deformation and propagation of the crack under the effect of the stress.

III 2 a Balancing :

In this stage, we observe a variation in the crystalline parameters for the predefined conditions required for tensile tests in the Oxy plane for temperatures ranging from 0 to 300 K for 30 seconds.

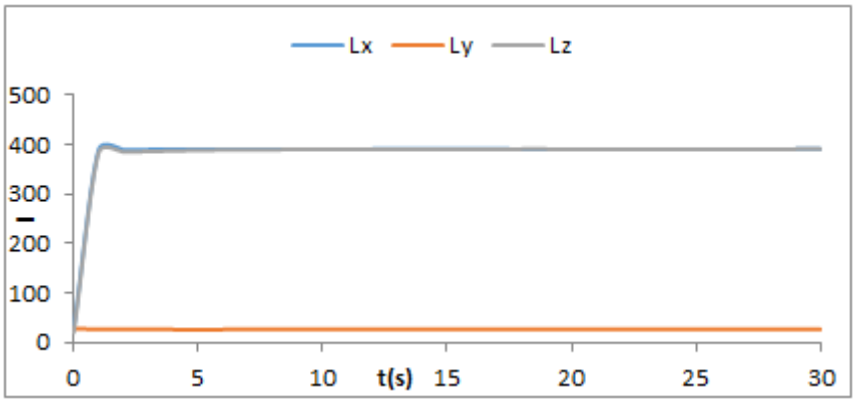

Figure 5: evolution of parameters during expansion vs. time

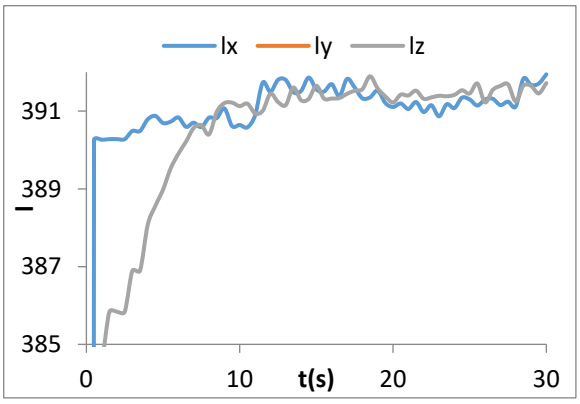

Figure 6: Lx, Ly and Lz parameters

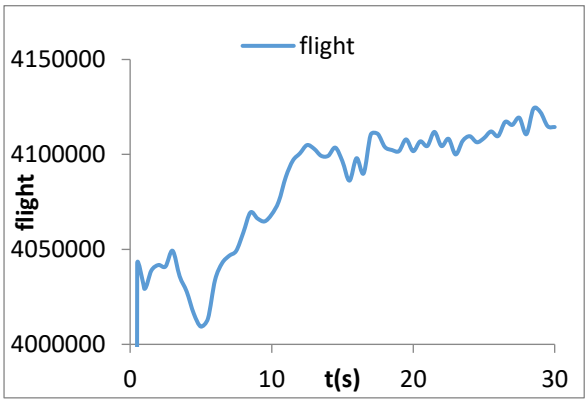

Figure 7: Volume expansion

ISSN: 2277-9655
Impact Factor: 5.164
CODEN: IJESS7

The variations are observed on (Ox) and (Oz) , These results clearly show that the volume increases during traction.

We then studied the behaviour of the physical quantities during this traction phase; these quantities are presented in the following figures :

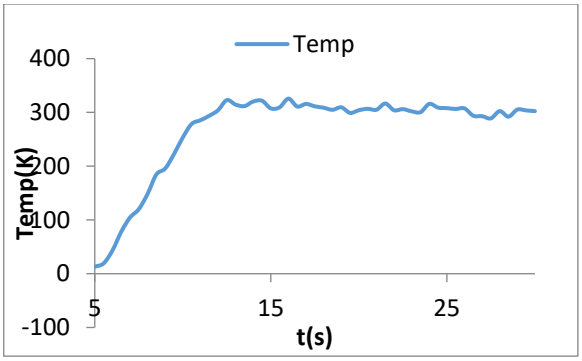

Figure 8: Temperature vs. time

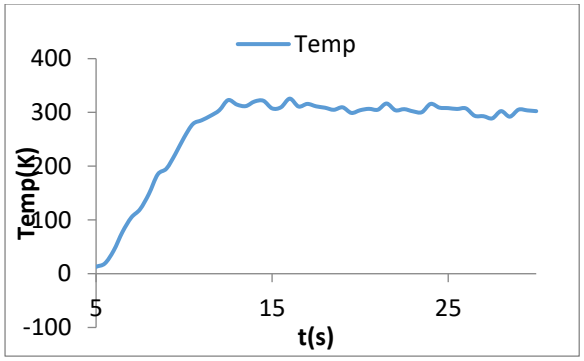

Figure 9: Temperature vs. cycle

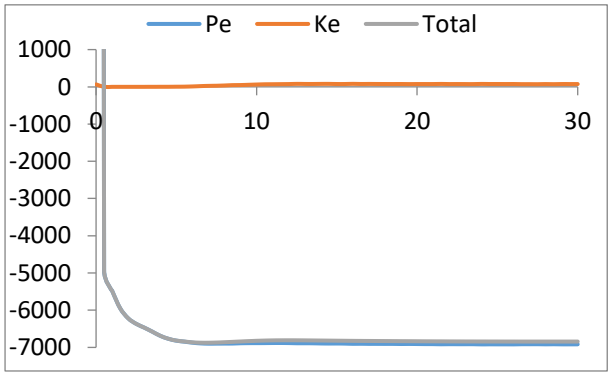

Figure 10: Energy behaviour vs. time

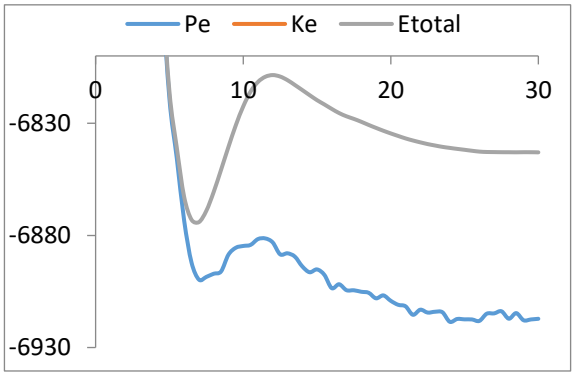

Figure 11: Total and potential energy vs. time

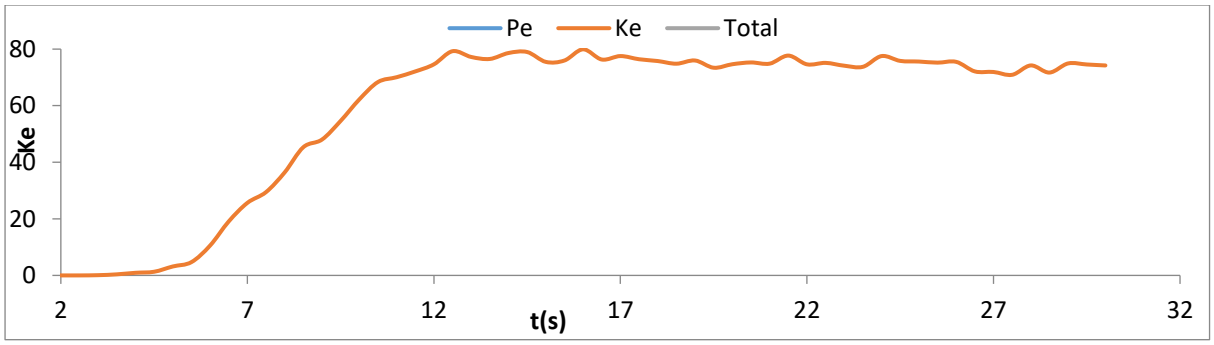

Figure 12: Evolution of kinetic energy

The temperature (and the kinetic energy of the particles) increases linearly, stabilising for the last 20 seconds at around 300 K, the period during which the structure would show a secondary stability revealed by the total energy.

- Observation shows that during the first 5 seconds, the material suffers no significant effect;

ISSN: 2277-9655
Impact Factor: 5.164
CODEN: IJESS7

- Between 5 and 12 seconds, expansion takes place and considerably affects the material, which sees its physical properties change considerably, although an exception is noted for Lx ;
- From 12 to 30 seconds, the temperature stops rising while reaching its maximum of 300°K.

III 2 b Strain: Effect of stress

Once the system has reached its steady state at around 300°K, we apply the following tensile stress (Oz) for the last 30 seconds, reaching its maximum value of 30 Gpa at around 60 seconds.

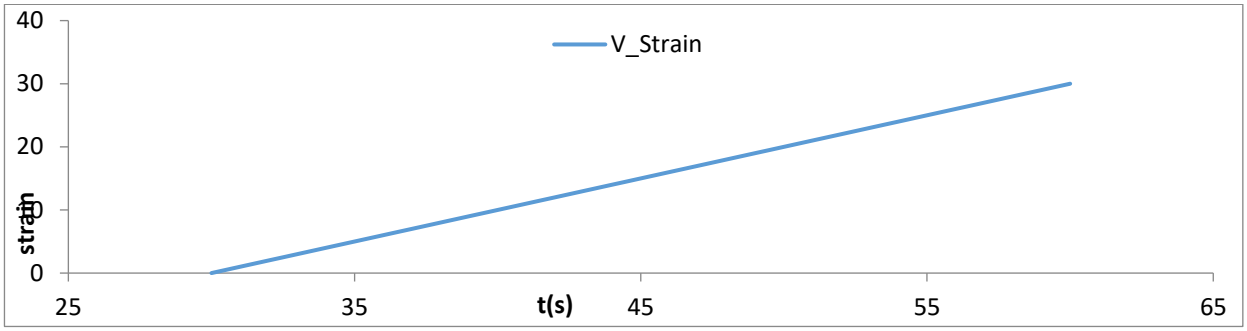

Figure 13: evolution of stress vs. time

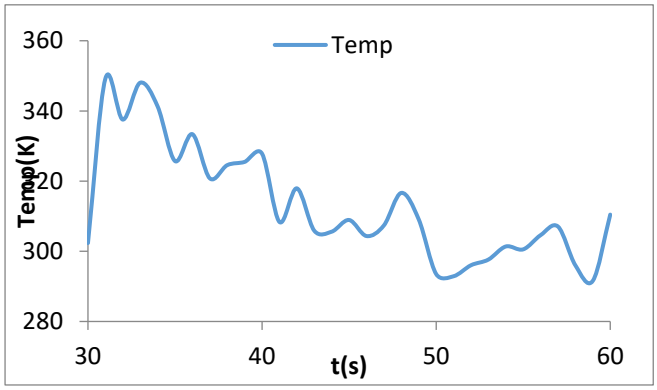

Figure 14: temperature vs. time

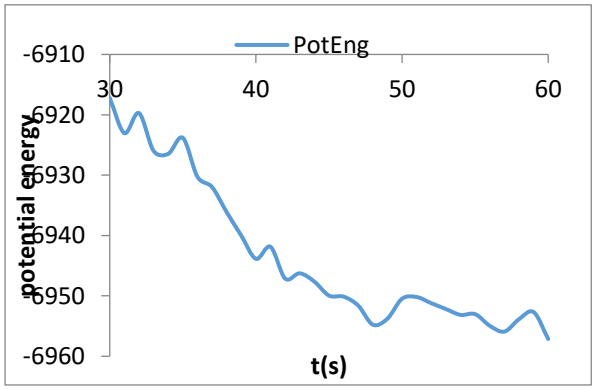

Figure 15: Potential vs. time

During this deformation, we observed :

- A drop in temperature of between 300 and 280 K over the last 30 seconds;
- Also noted a disorganisation (instability) of the structure, depending on the behaviour of the potential energy.

Other physical quantities were calculated during this deformation phase under the effect of stress.

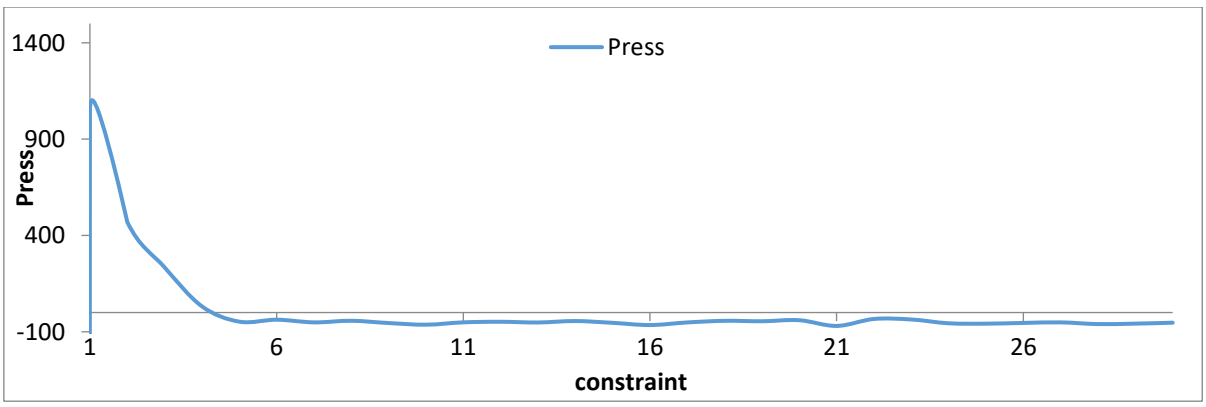

ISSN: 2277-9655
Impact Factor: 5.164
CODEN: IJESS7

Figure 16: overall pressure vs stress

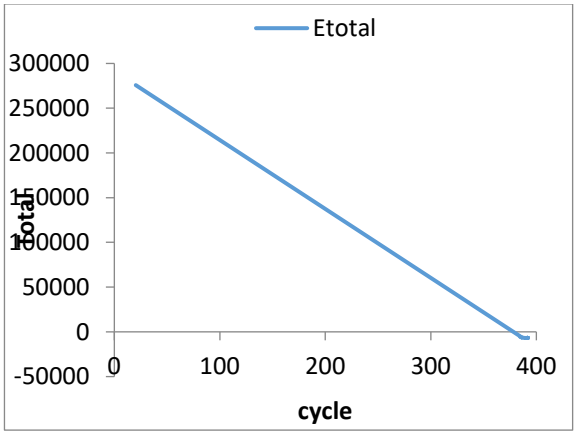

Figure 17: Energy drop vs. cycle

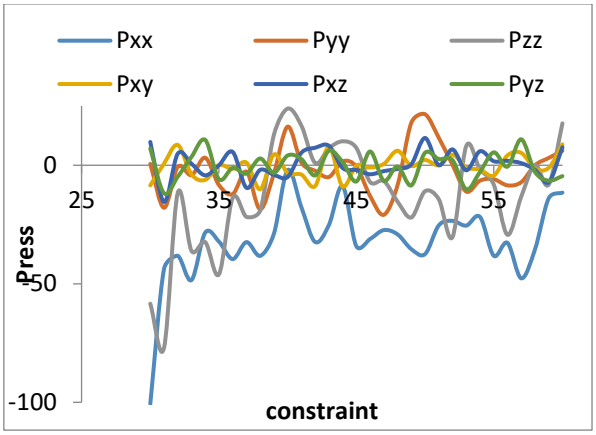

Figure 18: Pressure vs. stress

- We have noted here that the drop in total energy is crucial for the start of a crack;
- The behaviour observed on the different planes shows that the xx plane is the least affected and that the zz plane is the most affected; the crossed planes seem to be affected in the same way by the constraint ;
- The deformation is mainly felt on the axis (oy), which undergoes a contraction that reduces the value of y to reveal the cracking around the first 10 Gpa.

III 2 c Crack: crack propagation

We present here the behaviour of our material when subjected to the imposed stress. The results observed suggest ductile fracture.

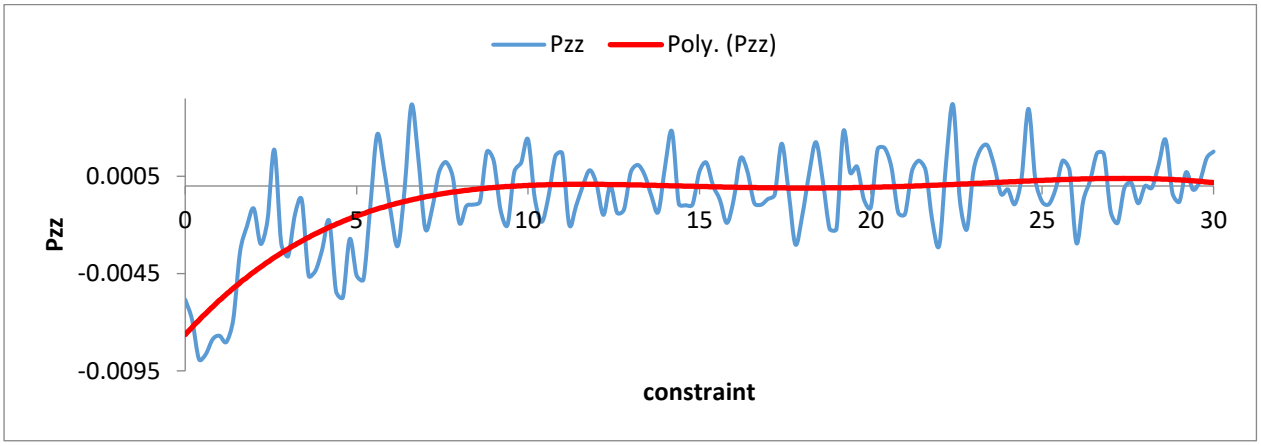

Figure 19: pressure vs. stress

ISSN: 2277-9655
Impact Factor: 5.164
CODEN: IJESS7

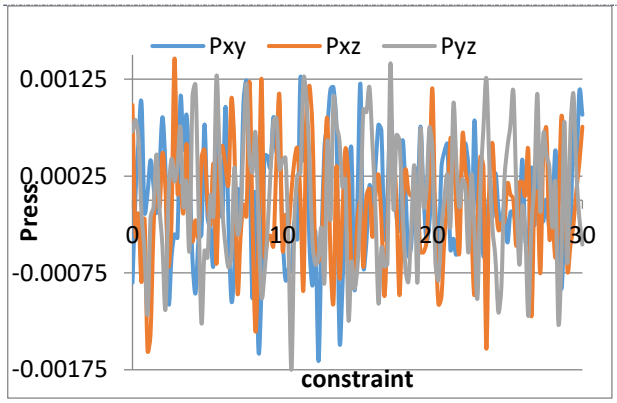

Figure 20: comparison of pressure vs. stress

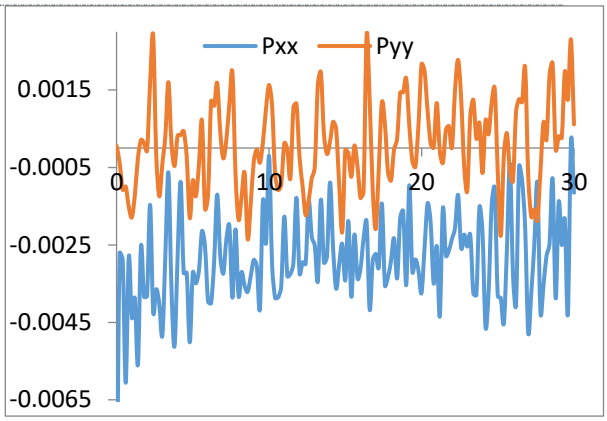

Figure 21: pressures (xx), (yy) vs stress

Trend observation, red curve,

- Between 0 and 5 Gpa, the behaviour of our material is elastic
- From 5 to 10 Gpa, elasticity reaches its maximum
- From 10 to 30 Gpa, the material is plastic,

Observation of the normal curve would suggest that the crack starts at around 5 Gpa, which is consistent with the behaviour observed on Oy.

Dans cette étape, l'évolution de la pression sur (oy) en fonction de la contrainte nous donne un résultat qui incarne bel et bien l'allure ductile de rupture. Cependant, la coordonnée en abscisse de la Figure3-16 diffère de celle utilisée dans la Figure 1-6. La procédure suivie dans cette étape pour parvenir à nos résultats est celle proposée dans [26]

III 3 Paris Law :

The data obtained during the deformation allowed us to apply the Paris law around 30 to 60 seconds. To do this, we used the trend curve for the behaviour of y (0y) to generate depth values based on the temperature behaviour of the material over the last thirty (30) seconds.

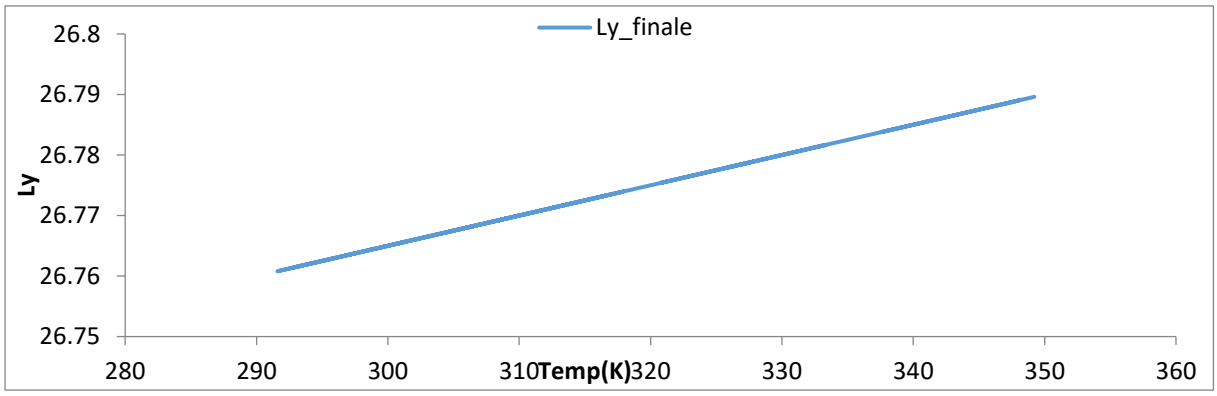

Figure 22: Behaviour of the mesh parameter vs temperature from 350- 300 °k

All the data that enabled us to apply the Paris law is shown in the table below:

Table 2: Parameter behaviour, Paris law

Crack propagation 30-60s		Paris Law C *10^9	
Temp K	**Ly_finale**	**Cycle**	**K**

ISSN: 2277-9655
Impact Factor: 5.164
CODEN: IJESS7

	(Generated)		
349,21532	***26,7896077***	*500*	***3759,600242***
337,53879	***26,7837694***	*1000*	***30076,80194***
348,04123	***26,7890206***	*1500*	***101509,2065***
341,29978	***26,7856499***	*2000*	***240614,4155***
325,71254	***26,7778563***	*2500*	***469950,0302***
333,3682	***26,7816841***	*3000*	***812073,6523***
320,78437	***26,7753922***	*3500*	***1289542,883***
324,55249	***26,7772762***	*4000*	***1924915,324***
325,47992	***26,77774***	*4500*	***2740748,576***
327,81657	***26,7789083***	*5000*	***3759600,242***
308,35906	***26,7691795***	*5500*	***5004027,922***
317,93925	***26,7739696***	*6000*	***6496589,218***
305,8589	***26,7679295***	*6500*	***8259841,732***
305,59119	***26,7677956***	*7000*	***10316343,06***
308,92365	***26,7694618***	*7500*	***12688650,82***
304,34575	***26,7671729***	*8000*	***15399322,59***
307,38781	***26,7686939***	*8500*	***18470915,99***
316,64649	***26,7733232***	*9000*	***21925988,61***
309,07999	***26,76954***	*9500*	***25787098,06***
293,52636	***26,7617632***	*10000*	***30076801,94***
292,88683	***26,7614434***	*10500*	***34817657,84***
296,02287	***26,7630114***	*11000*	***40032223,38***
297,63977	***26,7638199***	*11500*	***45743056,14***
301,37288	***26,7656864***	*12000*	***51972713,75***
300,55773	***26,7652789***	*12500*	***58743753,78***
304,60299	***26,7673015***	*13000*	***66078733,85***
307,04519	***26,7685226***	*13500*	***74000211,56***
295,97299	***26,7629865***	*14000*	***82530744,51***
291,59064	***26,7607953***	*14500*	***91692890,3***

To plot the betting law, we used an empirical method for choosing the parameters "**C**" and "**m**", which are very complex. However, knowing the extremes for C, we set it at **3.45 10-^{9}** , while for the value of "**m**'', we represented a set of curves while seeking the one closest to the Paris law.

ISSN: 2277-9655
Impact Factor: 5.164
CODEN: IJESS7

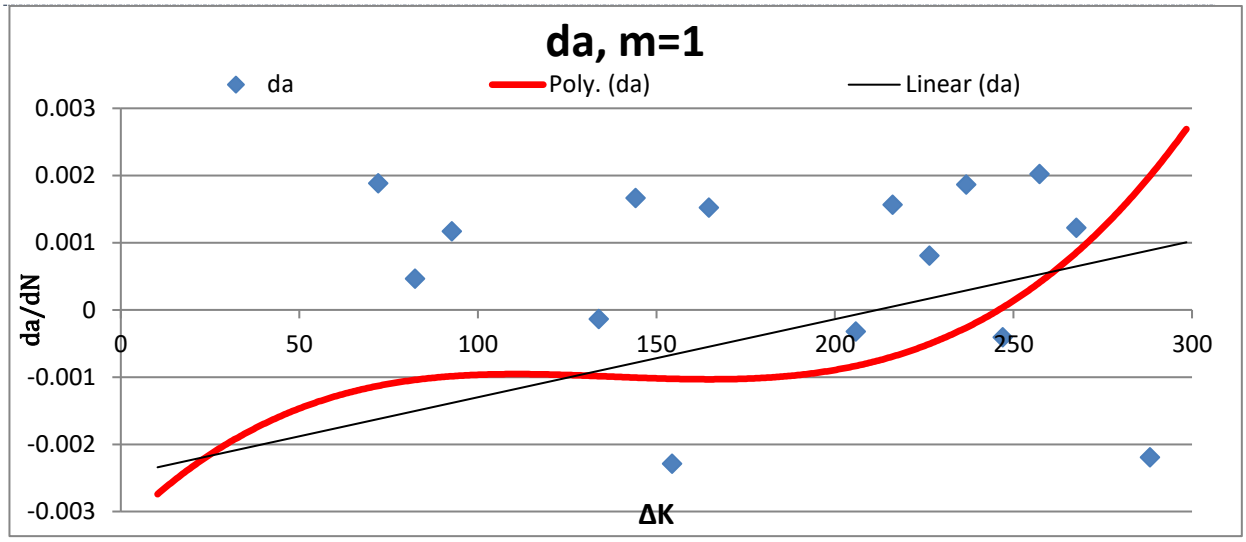

Figure 23: Cracking speed vs stress intensity factor (m=1)

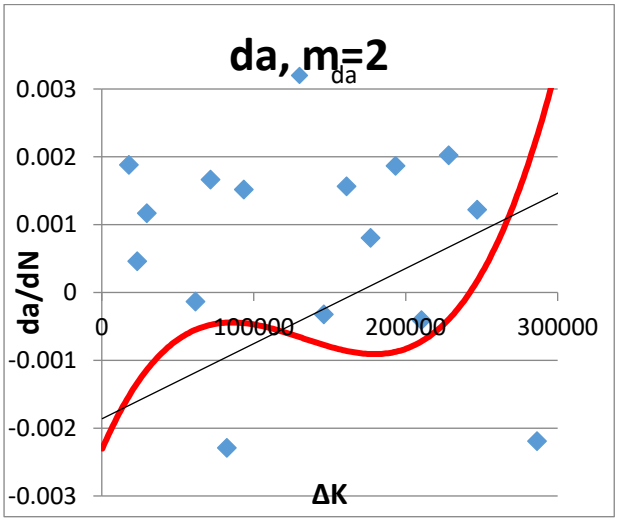

Figure24: speed vs FIC (m=2)

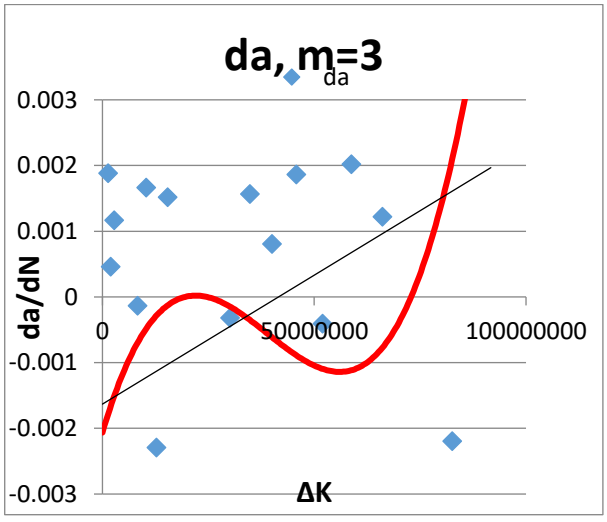

Figure25: speed vs FIC (m=3)

The curve obtained with m=1 gives a better approximation to the Paris law for the set value of "**C''.**

,

Figure 23 shows a typical curve for the *da/dN* propagation rate as a function of *ΔK*. Regardless of the curve observed, three propagation regimes can be distinguished.

- The first, **the threshold regime** (**regime I, from 0 to 100**), is characterised by the propagation threshold ΔK_{seuil} below which ***long cracks do*** not propagate. Several factors can influence the behaviour in **fatigue-propagation behaviour** near the threshold, such as the microstructure, the load ratio *R = Kmin /Kmax* and the mechanical properties (yield strength).

- The second, **the Paris regime** (**regime II, from 100 to 200**), concerns the stable propagation of long cracks and is often modelled by the Paris relation. The rate of propagation in this region can be influenced in particular by the load ratio, closure effects and loading frequency.
- The third, the accelerated propagation regime (regime III, from 200 to 300), is marked by an acceleration in the rate of propagation until the material gradually breaks down, where Kmax reaches the material's toughness KIc.

4. CONCLUSION

ISSN: 2277-9655
Impact Factor: 5.164
CODEN: IJESS7

In this work we studied the propagation of cracks in the B2 structure of NaCl-type Ti-Al found on the "materials projects" site with a mesh size of 10*10*10, i.e. for 2000 atoms. This study was made possible by using the MEAM potential of Ti-Al and the molecular dynamics incorporated in the LAMMPS calculation code.
All the stages of this study have just enabled us to empirically apply the Paris law while setting the parameter C at 3.45 10-9 and have revealed that :

- Cracking is the propagation of structural instability;
- Lowering the temperature around cracking ;
- The propagation regime ends with accelerated propagation.

Several studies can be carried out, in particular according to the three crack propagation regimes, to determine all the mechanical characteristics of the structure studied in order to improve its properties in the face of fracture:

- It is necessary to calculate the constants "C" and "m" specific to TiAl in order to better understand the normal mode of propagation of the crack;
- This study must be carried out on different faces for different crystallographic structures of TiAl.

This fragment should obviously state the foremost conclusions of the exploration and give a coherent explanation of their significance and consequence.

5. ACKNOWLEDGEMENTS

This section should be typed in character size 10pt Times New Roman, Justified.

REFERENCES

1. Xavier BIDAULT, 2007, Thesis to obtain the degree of Doctor of Physics: Etude par modélisation des nanoparticules formées par séparation de phases dans les verres dopés terre rare, p. 1-127
2. Mr Yves Alain BEH ONGUENG, 2013, PhD thesis from Pierre et Marie Curie University (Paris 6): Simulation atomistique Monte Carlo Cinétique des processus de croissance de couches passives sur alliages métalliques. Cas des alliages Fer-Chrome, p. 1-210.
3. Irwin, G.R. (1957), Analysis of stresses and strains near the end of a crack traversing a plate, Journal of Applied Mechanics, 24, 361-4.
4. [4] Paris, P.C., Gomez, M.P., Anderson W.P. (1961). A rational analytic theory of fatigue. The trend in engineering 13, pp. 528-34.
5. [5] N. MALESYS, S. POMMIER, Principaux mécanismes de fissuration par fatigue en mode I, 10/042009, Page 6 - 7
6. [6] S. Pommier, A study on the relationships between variable amplitude fatigue crack growth and the cyclic constitutive behaviour of an alloy, Int. J. Fatigue, in press.
7. [7] G.T. Hahn, Met Trans 3, p. 1192, 1972
8. [8] htpps:/nist.gov/